Geometry optimization and pressure analysis of a proton exchange membrane fuel cell stack

Wei-Hsin Chen [1,2,3,*], Zong-Lin Tsai [1,4], Min-Hsing Chang [5,*], Siming You [6], Pei-Chi Kuo [7]

1. Department of Aeronautics and Astronautics, National Cheng Kung University, Tainan 701, Taiwan
2. Research Center for Smart Sustainable Circular Economy, Tunghai University, Taichung 407, Taiwan
3. Department of Mechanical Engineering, National Chin-Yi University of Technology, Taichung, 411, Taiwan
4. International Master Degree Program on Energy Engineering, National Cheng Kung University, Tainan 701, Taiwan
5. Department of Mechanical Engineering, Tatung University, Taipei,104, Taiwan
6. James Watt School of Engineering, University of Glasgow, Glasgow, UK, G12 8QQ
7. Green Energy and Environment Research Laboratories, Industrial Technology Research Institute, Tainan 711, Taiwan

* Corresponding author; weihsinchen@gmail.com; chenwh@mail.ncku.edu.tw (W.H. Chen); mhchang@ttu.edu.tw (M.H. Chang)

Abstract

For proton exchange membrane fuel cells (PEMFCs), the distribution of reactant streams in the reactor is critical to their efficiency. This study aims to investigate the optimal design of the inlet/outlet flow channel in the fuel cell stack with different geometric dimensions of the tube and intermediate zones (IZ). The tube-to-IZ length ratio, the IZ width, and the tube diameter are adjusted to optimize the geometric dimensions for the highest pressure uniformity. Four different methods, including the Taguchi method, analysis of variance (ANOVA), neural network (NN), and multiple adaptive regression splines (MARS), are used in the analyses. The results indicate the tube diameter is the most impactive one among the three factors to improve the pressure uniformity. The analysis suggests that the optimal geometric design is the tube-to-IZ length ratio of 9, the IZ width of 14 mm, and the tube diameter of 9 mm with the pressure uniformity of 0.529. The relative errors of the predicted pressure uniformity values by NN and MARS under the optimal design are 1.62% and 3.89%, respectively. This reveals that NN and MARS can accurately predict the pressure uniformity, and are promising tools for the design of PEMFCs.

Keywords: Fuel cell stack; pressure uniformity; Taguchi method; Analysis of variance (ANOVA); Neural network (NN); Multivariate adaptive regression splines (MARS).

Nomenclature

$B_i(x)$	Basic function
C_0	Inertial resistance
C_i	Constant coefficient
D_ω	Cross-diffusion term
d	Penalizing parameter
E	Error function
$f(x_i)$	Predicted value
$\tilde{G}_k$	Generation of k
G_ω	Generation of ω
In	Inlet
K	Permeability
k	Turbulent kinetic energy
M	Number of BFs
N	Number of observations
Out	Outlet
P	Pressure (Pa)
ΔP_{total}	Total pressure drop (Pa)
ΔP_n	Pressure drop of the n^{th} cell (Pa)
ΔP_{inlet}	Pressure drop in the inlet channel (Pa)
ΔP_{outlet}	Pressure drop in the outlet channel (Pa)
$\vec{S}_k$	Source term
$\vec{S}_w$	Source term
T	Transpose matrix
Y_k	Dissipation of k

Y_ω	Dissipation of ω
y	Pressure uniformity
$\widehat{y_j}$	Output value
y_j	Desired output value.

Greek letters

γ	Porosity
$\vec{\tau}$	Stress tensor ($N \cdot m^{-2}$)
μ	Viscosity coefficient ($kg \cdot m^{-1} \cdot s^{-1}$)
μ_T	Scalar turbulence viscosity coefficient
ρ	Fluid density ($kg \cdot m^{-1}$)
ω	Specific dissipation rate
$\vec{v}$	Velocity vector ($m \cdot s^{-1}$)
σ_k	Closure coefficients of k
σ_ω	Closure coefficients of ω

1. Introduction

Proton exchange membrane fuel cells (PEMFCs) are a device that generates electricity and heat by the electrochemical reactions of hydrogen and air. Because of the high energy efficiency, no pollution, fast startup time, and low operation temperature, PEMFCs have been considered as a potential power source [1]. In practical applications, a PEMFC connects multiple cells into a stack to satisfy the required wattage supply. A lot of studies have been devoted to the analysis of flow field and flow channel design in the PEMFC system. Operating conditions, stack mechanisms, and uneven flow distributions all have great influences on the uniformity of the cell voltage [2-5]. Among these factors, the uniform distribution of the reaction gas in each cell is quite critical which can greatly improve the fuel cell efficiency and lifetime. Therefore, it is very important to understand the influence of flow uniformity on fuel cell efficiency and energy loss to improve fuel cell performance [6].

Many researchers have used the Taguchi method to study fuel cell effectiveness. The Taguchi method is an experimental method that can help the design of fuel cells by analyzing the effects of different factors. Accordingly, the most suitable or optimal design can be determined. This method can save a lot of time and cost which has been widely used in different research fields [7-10]. Wu et al. [11] combined the Taguchi method with the three-dimensional PEMFC model to achieve the optimal placement of rectangular cylinders in the channel. They also used the Taguchi method to find the best experimental combination of the factors and used the finite element method to simulate the migration phenomenon and electrochemical reaction. Karthikeyan [12] employed a standard orthogonal array of the Taguchi method and considered various landing-to-channel width ratios of the interdigitated flow channels to optimize the pressure and temperature distributions in the cell.

The Taguchi method can also be used together with the neural network (NN) in fuel cell research to reduce the number of experiments or simulations and achieve the goal efficiently

[13]. A well-designed NN model has excellent multi-dimensional mapping capabilities and can accurately represent the complex relationship between input and output spaces [14]. It has been extensively used in various research fields of science and technology. The combination of the Taguchi method and NN technology can successfully solve some problems that the Taguchi method fails to obtain the true optimal value when it is employed purely in the analysis [15, 16]. By the combination of the Taguchi method NN, Wu et al. [17] performed an analysis of PEMFC performance to determine the optimal operation parameters such as the operating temperature, pressure, and the flow rates of reactants. Chang et al. [18] used the same method with a numerical PEMFC model to predict the optimal working power of an unknown PEMFC. Chang [13] also combined the Taguchi method and the genetic algorithm NN model to propose a new method for estimating the output voltage of a PEMFC. Yu et al. [19] utilized the Taguchi method with NN to determine the maximum power output of a PEMFC from the experimental data.

Multivariate adaptive regression splines (MARS) is another commonly used classification technique in the research of data analysis. It is a nonlinear and nonparametric regression statistical method. This method does not need any assumption for the association between dependent and independent variables [20, 21], which can model nonlinearities and interactions between variables mechanically for higher-dimensional data analysis [22]. In some investigations, researchers have tried to combine MARS and neural networks in the analyses [23-25]. Adoko et al. [26] established a model that predicted the diameter convergence of a high-speed railway tunnel in the weak rock by the methods of MARS and artificial neural networks. Cheng et al. [27] built an evolutionary multivariate adaptive regression splines (EMARS) model which was a hybrid of MARS and artificial bee colony (ABC) to estimate the shear strength of reinforced concrete (RC) deep beams. Zhang et al. [28] successfully developed the backpropagation neural network (BPNN) and MARS models to assess pile drivability

concerning the maximum compressive stresses (MCS), maximum tensile stresses (MTS), and blow per foot (BPF).

So far the researches are quite limited about the effects of geometric dimensions of inlet and outlet flow channels of a PEMFC stack on its internal flow fields. At the same time, no researchers have applied the MARS to PEMFC. Therefore, this study aims to investigate the variation of the flow field in a fuel cell stack with different geometric dimensions of inlet and outlet channels by comprehensively combining computational fluid dynamics (CFD), Taguchi method, ANOVA, NN, and MARS. A stack consisting of 30 cells is considered to determine the optimal geometric sizes of the inlet and outlet channels for improving the pressure uniformity. The results can provide important insights and references for the promotion of fuel cell stack performance.

2. Mathematical formulation

2.1. Schematic of PEMFC stack model

The model of the PEMFC stack has 30 cells and consists of the tubes, intermediate zones (IZ), and inlet/outlet channels, as shown in **Fig. 1a**, in which the flow channels in the stack are approximated by porous zones. The porous medium model is used in the simulations since it can simulate the flow characteristics in the fuel cell stack efficiently without the loss of generality [29, 31-33], in which the permeability of porous medium can indicate the pressure drop in the flow channels. The tube and the IZ represent the end plate, as depicted in **Figs. 1c-d**, and the IZs at the inlet and outlet sections are expansive and contractive, respectively. The geometry of the tube and the IZs at the inlet and outlet sections are exactly equal. The thickness of each cell is 0.800 mm and the distance between adjacent cells is 0.635 mm. The three-dimensional fuel cell model was built by SolidWorks 2018. In the simulations, the internal fluid flow is assumed to be pure gas flow only, and the transport of liquid water is ignored. The effects of electrochemical reaction and heat transfer on the fluid flow are neglected for

simplification. The complicated texture of the flow channel is replaced by a narrow long straight plate and treated as porous medium zones.

2.2. Theoretical model and simulation

The gas flow is assumed to be incompressible turbulent flow because the Reynolds number in the flow channel is above 4000. The effect of gravity is ignored, and the no-slip condition is employed on the walls. The fuel cell stack is divided into two parts: the non-porous zones and the porous medium zones. The governing equations in the non-porous zones are [30]

$$\nabla \cdot (\rho \vec{v}) = 0 \tag{1}$$

$$\rho\, \vec{v} \cdot \nabla\, \vec{v} = -\nabla P + \nabla \cdot [\mu(\nabla\, \vec{v} + (\nabla\, \vec{v})^T)] \tag{2}$$

where ρ is the fluid density, $\vec{v}$ is the air velocity, P is the pressure, and μ is the viscosity. In the porous medium zones, the governing equations are [31, 32]

$$\nabla \cdot (\gamma \rho \vec{v}) = 0 \tag{3}$$

$$\nabla \cdot (\gamma \rho \vec{v} \vec{v}) = -\gamma \nabla P + \nabla \cdot (\gamma \vec{\tau}) - \left(\frac{\gamma^2 \mu}{K} \vec{v} + \frac{\gamma^3 C_0}{2} \rho |v| \vec{v} \right) \tag{4}$$

where γ is the porosity, $\vec{\tau}$ is the viscous stress tensor, μ is the viscosity, K is the permeability, and C_0 is the inertial resistance. Permeability and inertial resistance were obtained through a trial and error process from the experiment data correlating the pressure and volume flow rate. After trial and error, the permeability and inertial resistance are 9×10^8 and 100, respectively. In order to simulate the turbulent flow, the commercial software ANSYS 2019 R3 was used to perform the simulations in which the shear stress transport (SST) $k-\omega$ turbulence model was employed. The SST $k-\omega$ model has a similar form to the standard $k-\omega$ model and can solve transport equations for the turbulent kinetic energy k and the specific dissipation rate ω as follows:

$$\rho(\vec{v} \cdot \nabla)k = \nabla \cdot [(\mu + \mu_T \sigma_k)\nabla k] + \tilde{G}_k - Y_k + S_k \tag{5}$$

$$\rho(\vec{v} \cdot \nabla)\omega = \nabla \cdot [(\mu + \mu_T \sigma_\omega)\nabla \omega] + G_\omega - Y_\omega + D_\omega + S_w \tag{6}$$

In these equations, $\tilde{G}_k$ represents the generation of turbulence kinetic energy due to mean

velocity gradients, and G_ω stands for the generation of ω. Y_k and Y_ω are respectively the dissipation of k and ω due to turbulence, S_k and S_w are user-defined source terms, and D_ω is the cross-diffusion term.

The constants in the SST $k-\omega$ turbulence model were the same as the default values used in ANSYS 2019 R3. A pressure-based solver was chosen from the options offered in ANSYS, where a finite volume method was used to discretize the governing equations. A coupled scheme was utilized for pressure-velocity coupling calculations. The spatial discretization was conducted by the green-gauss node based on gradient and the second-order upwind method was used for solving the pressure and momentum. TC

The grid tests for the numerical results were carried out before executing simulations. Four grid numbers of Mesh 1 (329,755), Mesh 2 (551,904), Mesh 3 (756,032), and Mesh 4 (1,751,332) were tested, and the appropriate grid number was determined by comparing the volumetric flow rates at the inlet with the experimental data. For the case of a single cell, the simulation results were 0.197, 0.187, 0.183, and 0.180 L/min for the four grid numbers, respectively, and the experimental data was 0.186 L/min. The numerical results converged gradually with increasing grid number, while the time consumption increased greatly, especially for the case of Mesh 4. The results showed that Mesh 2 was sufficient to obtain a reasonable prediction with a relative error of less than 1% in comparison with the experimental data. The comparisons were also performed for the other three flow rates with excellent agreements, as illustrated in **Fig. 2**. For the case of a 10-cell stack, the measured flow rate was 4.85 L/min at the inlet pressure of 8.71 kPa. The simulation result was 5.32 L/min which was also in good agreement with a relative error of less than 10%. Similar results were also observed for the other three cases, as shown in **Fig. 2** at different flow rates. Accordingly, Mesh 2 was employed to perform the present simulations. The comparisons in **Fig. 2** also intrinsically fulfilled the numerical validation.

2.3. Taguchi method

The Taguchi method is an efficient and cost-saving technique for experiment design. It is characterized by an orthogonal array that screens the experiments to be performed without compromising any main or interacting effect of the parameters. The orthogonal array contains factors and levels, while the signal-to-noise ratio (S/N ratio) is made and used to assort the experimental results. Three different forms of S/N ratios, including the nominal-the-better (NB), the larger-the-better (LB), and the smaller-the-better (SB), are defined in the method [7]. The sensitivity of the parameters on the physical behavior can be figured out clearly by employing a parameter of signal-to-noise (S/N) ratio. In the S/N ratio, the signal represents the desired real value, while noise designates the undesired factors in measured values [10]. The objective of the present study is to maximize the pressure uniformity in the fuel cell stack. Thus, the LB criterion is adopted and the S/N ratio in terms of pressure uniformity is written as:

$$\frac{S}{N} = -10\log_{10}\left(\frac{1}{y^2}\right) \tag{7}$$

where y is a dimensionless value which means the pressure uniformity in the fuel cell stack, and is defined as [33]

$$y = \frac{\Delta P_n}{\Delta P_{total}} = \frac{\Delta P_{total} + \Delta P_{inlet} - \Delta P_{outlet}}{\Delta P_{total}} = 1 + \frac{\Delta P_{inlet} - \Delta P_{outlet}}{\Delta P_{total}} \tag{8}$$

where ΔP_n is the pressure drop of the nth cell in the stack, ΔP_{total} is the total pressure drop of the stack, ΔP_{inlet} is the pressure drop in the inlet channel, and ΔP_{outlet} is the pressure drop in the outlet channel.

The pressure drop affects the pressure uniformity and can be used to evaluate the fluid flow distribution within the channel qualitatively [33]. Thus, pressure uniformity for optimization is used instead of flow distribution, while they both may result in the same result. According to the definition of **Eq. (8)**, the ideal pressure uniformity should approach one as close as possible.

2.4. Operating conditions

In the design of the tube and IZ, three control factors are considered: the tube-to-IZ length

ratio, the IZ width, and the tube diameter, as shown in **Fig 1b**, which are denoted by Factors A, B, and C, respectively. The ranges of sizes for designing the geometry of the tube and IZ are based on the practical sizes of PEMFC. The total length of the tube and IZ are 140 mm, and the IZ length is no more than 40 mm. The IZ width is less than 20 mm of the width of the inlet/outlet channel. The tube diameter is 12 mm which is less than the height of the inlet/outlet channel. Each factor consists of four levels as listed in **Table 2**. For the Taguchi method, a typical orthogonal array L_{16} (3^4) with 16 runs is given in **Table 3**.

2.5. Data analysis

The required network can be acquired using the neural network (NN) in the prediction function, and the multivariate adaptive regression splines (MARS) models are calculated with the regression function of the software PolyAnalyst 6.0.

2.5.1. Neural network (NN)

NN is a non-linear statistical data modeling instrument. It is usually optimized through a learning method based on mathematical statistics. There are many kinds of NN [34]. The backpropagation neural network (BPNN) was employed in this study. The BPNN is an algorithm for error backpropagation training with a multi-layer network structure that has three layers of network configuration: an input layer, a hidden layer, and an output layer. It is mainly composed of two stages which are the activation function and the update of weight values. The BPNN is fitted using the steepest descent method and the network connection weight values and thresholds are automatically adjusted by the backpropagation of the output error. Accordingly, the desired error could be achieved by minimizing the error value of the network. It aims to learn the parameters that can minimize the mean square error, and the defined error function E is expressed as [35, 36]

$$E = \frac{1}{2}\sum_{j=1}^{l}\left(\hat{y}_j - y_j\right)^2 \tag{9}$$

where $\hat{y}_j$ is the output value and y_j is the target value. The brief procedures are described as

follows [37] and also in the flowchart shown in **Fig. 3**:

I. Compare the output data with the target value and calculate the error in each neuron.

II. For each neuron, determine how much the output must be adjusted to be lower or higher to match the target value.

III. Modify the weight value of each neuron to correct errors and improve accuracy.

IV. Give high importance to neurons connected by the stronger weight value.

V. Repeat the above steps until the final output error reached the target value.

2.5.2. Multivariate adaptive regression splines (MARS)

MARS is a well-known nonparametric regression method proposed by Friedman [38]. In comparison with the linear regression model, MARS can model nonlinearities and interactions between variables automatically. The MARS model is built into a spline in multi-dimension space and the spline is a continuous piecewise polynomial function [39]. It is expressed by a weighted value of basic functions (BFs) as the following equation

$$f(x_i) = \sum_{i=1}^{k} C_i B_i(x) \ , \tag{10}$$

where k is the total number of terms in the function, C_i is a constant coefficient estimated by the least-squares method, and $B_i(x)$ is the basic function. The BFs usually contains three items. One is the constant coefficient, another is a hinge function such as max (0, x-constant) or max (0, constant-x), and the other is the product of two or more hinge functions. The notation max$(\cdot,\cdot)$ denotes the maximum of two given values and x is the knot. MARS builds a model in two phases. In the first step, the knot in a hinge function is selected from the predictor values of observations which are assumed to be a set of candidate knots. MARS gradually adds suitable knots and the candidate knot that minimizes the fitting error is the most suitable knot in each round of knot addition. At the end of the first step, it usually builds an overfitted model that has a good fit to build the model but does not generalize well to new data. Therefore, the second step is to prune redundant BFs in the overfitted model. The generalized-cross-validation (GCV) technique is used to delete the BFs that supplies the lowest contributions. The GCV formula is

$$\mathrm{GCV} = \frac{\frac{1}{N}\sum_{i=1}^{N}[y_i f(x_i)]^2}{\left[1 - \frac{M + d \times (M-1)/2}{N}\right]^2} \quad (11)$$

where M is the number of BFs, N is the number of observations, d is the penalizing parameter, and $f(x_i)$ is the predicted value. Accordingly, the GCV value influences the number of BFs along with the number of knots and can reduce model overfitting. The relative importance of the factor can be produced by observing the GCV reduction when a factor is removed from the model after the model is determined.

3. Results and discussion

3.1. Factor analysis in the Taguchi method

The pressure uniformity profile for the 16 cases in **Table 3** is shown in **Fig. 4a**, and the simulation results are carried into the Taguchi optimization method. The results show that Case 7 has the highest pressure uniformity of 0.5224, whereas Case 16 has the lowest pressure uniformity of 0.375. **Eq. (7)** is used to determine the signal-to-noise (S/N) ratio of each case, and the S/N ratios of Case 7 and Case 16 are -5.6406 and -8.5191, respectively. The S/N ratios of the 16 cases are shown in **Fig. 4b**, while the distributions of the mean S/N ratios of the three factors in different levels based on **Table 2** are shown in **Fig. 4c**. Consider the mean S/N ratio of Factor A in Level 1, its value is the average of the S/N ratio for Factor A at Level 1, namely, the average of -8.0501 (Case 1), -7.1649 (Case 2), -6.5507 (Case 3), and -5.7052 (Case 4) [10]. Factors B and C at each level follow the same step to obtain the mean S/N ratios. The sensitivity of the pressure uniformity to the three factors within the investigated levels can be figured out by the maximum mean S/N ratio of the factor minus the minimum one, namely, the effect. A higher effect value of a factor implies the role played by the factor is more significant on the pressure uniformity because of the higher sensitivity of the pressure uniformity to the factor variation. The radar chart of the effect values of the three factors is shown in **Fig. 5a**. It depicts that the effect values are ranked by the tube diameter (Factor C, 2.688) > the tube-to-IZ length

ratio (Factor A, 0.213) > the IZ width (Factor B, 0.142). This implies that the IZ width almost plays no role in the pressure uniformity due to its very small effect value.

3.2. Analysis of variance (ANOVA)

ANOVA analysis is generally used to estimate and test the influence of the different factors. Here ANOVA is used to identify the important factor that could affect the pressure uniformity. The results of ANOVA are shown in **Table. 4**. The F value in ANOVA is the variance of the group means divided by the mean of the within-group variances. The higher the F value of the factor is, the greater the impact of the object value is [7]. From the critical value table of F_α (α is the false-rejection probability) under 3° of freedom of sum of the square of treatment, and 12° of freedom of sum of the square of error, it gives $F_{0.1} = 2.61$, $F_{0.05} = 3.49$, and $F_{0.01} = 5.95$. Accordingly, the conditions of $F < 2.61$, $2.61 < F < 3.49$, and $F > 5.95$ designate slight, mild, and high significant influences, respectively. The F value of Factor C is 2434.73 which is the highest among the three factors. This reflects that the tube diameter has a large influence on the pressure uniformity. The F values of Factors A and B are 19.15 and 4.0, respectively, indicating that their influence on the pressure uniformity is slight and mild. For the order of factor effect, it is the same as the Taguchi method, that is, the tube diameter (Factor C, 2434.73) > the tube-to-IZ length ratio (Factor A, 19.15) > the IZ width (Factor B, 4.0). The difference between the results of the Taguchi method and ANOVA analysis is the importance of factor C to the pressure uniformity. In the Taguchi method, only Factor C is more important than Factor A. However, the effect of Factor C is far more important than Factors A and B in ANOVA analysis.

3.3. Optimal combination

The optimal combination of the three factors to pressure uniformity can be determined from the results shown in **Table 4** and **Fig. 4c**. Scilicet, the tube-to-IZ length ratio is 9 (Level 1), the IZ width is 14 mm (Level 1), and the tube diameter is 9 mm (Level 4). This combination is not included in the orthogonal array of the Taguchi method (**Table 3**), so the simulation for this combination is performed additionally. The simulation result of the pressure uniformity for

this combination is found to be 0.529. Comparing with all other cases in **Fig. 4a**, this combination exhibits the optimal operation in the 16 cases. Therefore, the use of the Taguchi method in optimizing the operating parameters for maximizing the pressure uniformity shows valuable results. Comparing with Case 7 which is the best operation in the 16 cases, the pressure uniformity can be enhanced. Among the 16 cases of the orthogonal array, Case 16 has the lowest pressure uniformity in comparison with the optimal combination recommended by the Taguchi method.

The optimal case is compared with Case 16 to find the difference in the physical phenomenon. The velocity contours of the two cases are shown in **Figs. 6a-b**, and the corresponding pressure contours are shown in **Figs. 6c-d**. Furthermore, the detailed pressure and mean velocity profiles along the inlet and outlet channels are shown in **Fig. 7**. In these two cases, the highest pressure occurs at the end of the inlet channel, whereas the lowest pressure occurs at the front end of the outlet channel. The total pressure drop of Case 16 is smaller than that of the optimal case. In the inlet channel, the pressure gradually increases, while it decreases gradually in the outlet channel. The velocity distribution depends on the pressure distribution in the inlet and outlet channel. The highest velocity occurs in the outlet area for all configurations, while the lowest velocity occurs in the dead-end area.

The flow patterns of the inlet and outlet channels of the two cases are compared and illustrated. The top and side views of the inlet channel are shown in **Fig. 8**, and those of the outlet channel are shown in **Fig. 9**. As shown in **Fig. 8**, when the flow enters the IZ from the tube, stronger recirculation zones in Case 16 are observed because its IZ is longer and the tube diameter is smaller than the width of IZ. This reduces the magnitude of fluid flow into the peripheral IZ. The large recirculation zones may redirect the fluid affecting the wall. There is an obvious vortex located at the intersection of the tube and the IZ. It causes an unstable flow in the IZ and affects the flow at the extremity of the inlet channel [40]. For the optimal case, the tube diameter is closer to the IZ width, so only small recirculation zones occur in the inlet

channel. The fluid flowing towards the IZ shows smaller recirculation zones and backflow. A similar situation was also found where the proper flared tube design could improve the uniformity of the airflow [41]. For the top and side view of the outlet channel in **Fig. 9**, it is noticed that the flow field in the outlet channel is not uniform due to the presence of recirculation zones in the vicinity of some outlets of cell channels [42]. When the fluid enters the outlet channel, the distribution is less uniform in Case 16. This arises from the fact that the fluid is dispersed into the recirculation zones when entering the IZ from the tube. Therefore, the velocity of the fluid entering the end of the stack decreases. It leads to an unevenly distributed fluid flow at the extremity of the channel when the fluid is flowing from the cell channel to the outlet channel. Compare with Case 16, due to the smaller recirculation zones in the optimal case, the fluid flow is more concentrated when it enters the stack and can be effectively transferred to the extremity of the channel. Therefore, when the fluid flow enters the outlet channel from the inlet channel, it is more concentrated and stable.

3.4. Data analysis in NN and MARS

The database for the data analysis is the results obtained by the Taguchi method, and the data are divided into training data and test data of 70% and 30%, respectively. The tube diameter, the tube-to-IZ length ratio, and the IZ width are set to the three input parameters, and the pressure uniformity is set to the output parameter. In practice, the training algorithm uses a one-layer network with resilient propagation (RPROP) [43], and the Elliot function [44] and the layer Sigmoid are used in the hidden layer and output layer, respectively. **Fig. 10a** shows the architecture of the neural network to illustrate the different geometry of the inlet channels for the pressure uniformity. The training process in NN stops when the error value between training and validation data is less than 0.005. As shown in **Fig. 10b**, the training at 200 consecutive epochs stops when the error value between training and validation data is less than 0.005. The regression plots of the NN model with 35 hidden neurons are shown in **Fig. 11a**. One can see a good fit between the predicted outputs and the targets (actual outputs) during training phases

364 with an NN model. The coefficient of determination (R^2) between the predicted outputs and the
365 targets is 0.975. The sensitivity of the three factors in NN is shown in **Fig. 5b**. The order of the
366 importance of the three factors is the tube diameter (Factor C, 0.62) > the tube-to-IZ length ratio
367 (Factor A, 0.201) > the IZ width (Factor B, 0.179). This order is in line with that of the Taguchi
368 method.

369 For the analysis of MARS, its model and the basic functions (BFs) for predicting the
370 pressure uniformity are listed in **Table 5**. Some BFs include two splines functions which
371 indicate the model can disclose the interactions. These interactions are the most important part
372 of the generation of an accurate model to estimate the pressure uniformity in the PEMFC [26].
373 The obtained MARS model is

$$\begin{aligned} y = {} & 0.3831 + 0.0140 \times BF_1 - 0.0028 \times BF_2 + 0.1572 \times BF_3 \\ & -0.0451 \times BF_4 - 0.0047 \times BF_5 + 0.0071 \times BF_6 + 0.0125 \times BF_7 \\ & -0.0775 \times BF_8 - 0.0479 \times BF_9 \end{aligned} \quad (9)$$

374 **Fig. 11b** shows a good fit between the predicted output of the MARS model during training and
375 the target (actual output). The R^2 value between the predicted outputs and the targets is 0.943.
376 The relative importance of the input variables considered in this MARS model is shown in **Fig.**
377 **5c**. Using the GCV value, the relative importance by removing the specified variable from the
378 MARS model can be evaluated. The results show that the influences of the factors are ranked
379 by the tube diameter (Factor C, 0.47) > the tube-to-IZ length ratio (Factor A, 0.45) > the IZ
380 width (Factor B, 0.07). The values reflect that the tube diameter and the tube-to-IZ length ratio
381 are relatively important parameters in the consideration of stack design. This rank also conforms
382 with those of the Taguchi method and NN.

383 Although the optimal combination has been found in the Taguchi method, it should be
384 noted that the best-operating conditions may not be on the selected four levels. Therefore, the
385 interval between each level can be divided into more levels, and the actual optimal combination
386 can be determined more accurately [17]. In the Taguchi method, there are only four levels for

387 the three factors. In contrast, NN can further partition the four levels into more values and find
388 the combinations that Taguchi does not consider. Accordingly, the four levels of the three factors
389 in the Taguchi method are extended to seven levels in this study. Specifically, in NN, the seven
390 levels of the tube-to-IZ length ratio include 9.0, 7.0, 5.7, 4.7, 4.0, 3.4 and 3.0, the levels of the
391 IZ width consist of 14.0, 14.5, 15.0, 15.5, 16.0, 16.5, and 17.0 mm, and the levels of the tube
392 diameter comprise 7.50, 7.75, 8.00, 8.25, 8.50, 8.75, and 9.00 mm. In **Figs. 12a-c**, three IZ
393 widths of 14.0, 15.5, and 17 mm are selected, and the pressure uniformity of each case is drawn
394 into a three-dimensional graph for comparison. The results of NN show that the tube diameter
395 has the greatest influence on the pressure uniformity of the fuel cell stack. The impacts of the
396 tube-to-IZ length ratio and the IZ width on the pressure uniformity are subtle which exhibits no
397 obvious change. The black dot in **Fig. 12a** is the highest uniformity and the optimal combination
398 is recommended by NN. Similarly, in MARS the three parameters are expanded to more levels.
399 **Figs. 13a-c** also shows the pressure uniformity distributions at the IZ widths of 14, 15.5, and
400 17 mm in MARS. The result shows that when the tube diameter or the tube-to-IZ length ratio
401 increases, the pressure uniformity increases. Once the IZ width increases, all areas with higher
402 uniformity decreases. It can also be seen that the tube diameter is still the most influential factor
403 on the pressure uniformity.

404 **Table 6** compares the results of the Taguchi method, NN, and MARS. The sensitivity
405 analysis points out that the tube diameter is the key factor in affecting the pressure uniformity.
406 The three different methods all suggest that the optimal combination is the tube-to-IZ length
407 ratio of 9, the IZ width of 14 mm, and the tube diameter of 9 mm. NN and MARS also predict
408 the pressure uniformity under the optimal combination, and their relative errors between the
409 predictions and the simulation are 1.62 % and 3.89 %, respectively, showing that both NN and
410 MARS can successfully predict the pressure uniformity in the fuel cell stack.

411 ## 4. Conclusions

412 The optimal design of tube and intermediate zones for a PEM fuel cell stack with 30 cells
413 has been investigated in this work. The influences of the tube-to-IZ length ratio, the IZ width,
414 and the tube diameter on the pressure uniformity in the fuel cell stack have also been analyzed
415 using the Taguchi method, neural network (NN), and multiple adaptive regression splines
416 (MARS). The results of the Taguchi method show that the importance of the three factors based
417 on their impacts on the pressure uniformity follows the order of the tube diameter, the tube-to-
418 IZ length ratio, and the IZ width. It is found that the pressure distribution presents the highest
419 uniformity under the combination of the tube-to-IZ length ratio of 9, the IZ width of 14 mm,
420 and the tube diameter of 9 mm. In the Taguchi method, the F value of ANOVA also shows that
421 the tube diameter is the most influential factor where a larger tube diameter and a smaller IZ
422 width give rise to smaller recirculation zones and relatively stable fluid flow. Besides, a longer
423 tube length can minimize the recirculation zones when the fluid flow enters the IZ. Hence, the
424 recommended geometric dimensions of the Taguchi method intensify the pressure uniformity
425 because the recirculation zones tend to be narrow and the vortex weakens. The influences of
426 the three factors on the pressure uniformity analyzed by NN and MARS also suggest the same
427 rank and optimal geometry as the Taguchi approach. The relative errors between the optimal
428 predicted pressure uniformity of NN and MARS and the simulation result are 1.62 % and 3.89
429 %, respectively, suggesting that NN and MARS are suitable tools in predicting the pressure
430 uniformity in the fuel cell stack and thereby the fuel cell design. Overall, the present work
431 benefits the data analysis from CFD results for the exploration of physical phenomena in
432 PEMFC which could save the time and cost of simulation in the future.

433 **Acknowledgments**

434 The authors acknowledge the financial support of the Ministry of Science and Technology,
435 Taiwan, R.O.C., under the contract numbers of MOST 108-2221-E-006-127-MY3, MOST 109-
436 2622-E-006-006-CC1, and MOST 109-3116-F-006-016-CC1 for this research.

References

[1] Liu S, Chen T, Zhang C, Xie Y. Study on the performance of proton exchange membrane fuel cell (PEMFC) with dead-ended anode in gravity environment. Applied Energy. 2020;261:114454.

[2] Qin Y, Du Q, Fan M, Chang Y, Yin Y. Study on the operating pressure effect on the performance of a proton exchange membrane fuel cell power system. Energy Conversion and Management. 2017;142:357-65.

[3] Fan L, Zhang G, Jiao K. Characteristics of PEMFC operating at high current density with low external humidification. Energy Conversion and Management. 2017;150:763-74.

[4] Shao H, Qiu D, Peng L, Yi P, Lai X. In-situ measurement of temperature and humidity distribution in gas channels for commercial-size proton exchange membrane fuel cells. Journal of Power Sources. 2019;412:717-24.

[5] Park J, Li X. Effect of flow and temperature distribution on the performance of a PEM fuel cell stack. Journal of Power Sources. 2006;162:444-59.

[6] Huang F, Qiu D, Lan S, Yi P, Peng L. Performance evaluation of commercial-size proton exchange membrane fuel cell stacks considering air flow distribution in the manifold. Energy Conversion and Management. 2020;203:112256.

[7] Chen W-H, Lin Y-Y, Liu H-C, Baroutian S. Optimization of food waste hydrothermal liquefaction by a two-step process in association with a double analysis. Energy. 2020;199:117438.

[8] Chen WH, Chen CJ, Hung CI. Taguchi approach for co-gasification optimization of torrefied biomass and coal. Bioresour Technol. 2013;144:615-22.

[9] Chen W-H, Chen C-Y, Huang C-Y, Hwang C-J. Power output analysis and optimization of two straight-bladed vertical-axis wind turbines. Applied Energy. 2017;185:223-32.

[10] Wu W, Lin M-H, Chen W-H. Exergy analysis of an EFC/PV/Battery-based hybrid power generation system. International Journal of Energy Research. 2015;39:406-17.

[11] Wu H-W, Ku H-W. The optimal parameters estimation for rectangular cylinders installed transversely in the flow channel of PEMFC from a three-dimensional PEMFC model and the Taguchi method. Applied Energy. 2011;88:4879-90.

[12] Lakshminarayanan VR, Karthikeyan P, Aswin C, Charandeep Singh DS. Parametric analysis of proton exchange membrane fuel cell (PEMFC) performed by the Taguchi method. Transactions of FAMENA. 2015;39:79-88.

[13] Chang K-Y. The optimal design for PEMFC modeling based on Taguchi method and

genetic algorithm neural networks. International Journal of Hydrogen Energy. 2011;36:13683-94.

[14] A.U. Levin KSN. Control of nonlinear dynamical systems using neural networks – part II: observability, identification, and control. IEEE Transactions on Neural Networks. 1996:30-42.

[15] Wang G-J, Tsai J-C, Tseng P-C, Chen T-C. Neural-Taguchi method for robust design analysis. 1998;19:223-30.

[16] Lin H-L, Chou C. Optimisation of the GTA welding process using the Taguchi method and a neural network. Science and Technology of Welding & Joining. 2006;11:120-6.

[17] Wu S-J, Shiah S-W, Yu W-L. Parametric analysis of proton exchange membrane fuel cell performance by using the Taguchi method and a neural network. Renewable Energy. 2009;34:135-44.

[18] Chang K-Y, Lin H-J, Chen P-C. The optimal performance estimation for an unknown PEMFC based on the Taguchi method and a generic numerical PEMFC model. International Journal of Hydrogen Energy. 2009;34:1990-8.

[19] Yu W-L, Wu S-J, Shiah S-W. Experimental analysis of dynamic characteristics on the PEM fuel cell stack by using Taguchi approach with neural networks. International Journal of Hydrogen Energy. 2010;35:11138-47.

[20] Zheng G, Yang P, Zhou H, Zeng C, Yang X, He X, et al. Evaluation of the earthquake induced uplift displacement of tunnels using multivariate adaptive regression splines. Computers and Geotechnics. 2019;113:103099.

[21] Zheng G, Zhang W, Zhou H, Yang P. Multivariate adaptive regression splines model for prediction of the liquefaction-induced settlement of shallow foundations. Soil Dynamics and Earthquake Engineering. 2020;132:106097.

[22] Lokuge W, Wilson A, Gunasekara C, Law DW, Setunge S. Design of fly ash geopolymer concrete mix proportions using Multivariate Adaptive Regression Spline model. Construction and Building Materials. 2018;166:472-81.

[23] Chou S-M, Lee T-S, Shao YE, Chen IF. Mining the breast cancer pattern using artificial neural networks and multivariate adaptive regression splines. Expert Systems with Applications. 2004;27:133-42.

[24] Lee T, Chen I. A two-stage hybrid credit scoring model using artificial neural networks and multivariate adaptive regression splines. Expert Systems with Applications. 2005;28:743-52.

[25] Lu C-J, Lee T-S, Lian C-M. Sales forecasting for computer wholesalers: A comparison of

multivariate adaptive regression splines and artificial neural networks. Decision Support Systems. 2012;54:584-96.

[26] Adoko A-C, Jiao Y-Y, Wu L, Wang H, Wang Z-H. Predicting tunnel convergence using Multivariate Adaptive Regression Spline and Artificial Neural Network. Tunnelling and Underground Space Technology. 2013;38:368-76.

[27] Cheng M-Y, Cao M-T. Evolutionary multivariate adaptive regression splines for estimating shear strength in reinforced-concrete deep beams. Engineering Applications of Artificial Intelligence. 2014;28:86-96.

[28] Zhang W, Goh ATC. Multivariate adaptive regression splines and neural network models for prediction of pile drivability. Geoscience Frontiers. 2016;7:45-52.

[29] Chen W-H, Tsai Z-L, Chang M-H, Hsu T-H, Kuo P-C. Flow field simulation and pressure drop modeling by a porous medium in PEM fuel cells. International Journal of Energy Research. 2021; https://doi.org/10.1002/er.6047.

[30] Chen W-H, Lin Y-X, Chiou Y-B, Lin Y-L, Wang X-D. A computational fluid dynamics (CFD) approach of thermoelectric generator (TEG) for power generation. Applied Thermal Engineering. 2020;173:115203.

[31] Zhong W, Xu K, Li X, Liao Y, Tao G, Kagawa T. Determination of pressure drop for air flow through sintered metal porous media using a modified Ergun equation. Advanced Powder Technology. 2016;27:1134-40.

[32] Chen W-H, Tsai C-W, Lin Y-L, Chein R-Y, Yu C-T. Reaction phenomena of high-temperature water gas shift reaction in a membrane reactor. Fuel. 2017;199:358-71.

[33] Chen C-H, Jung S-P, Yen S-C. Flow distribution in the manifold of PEM fuel cell stack. Journal of Power Sources. 2007;173:249-63.

[34] Özçelep Y, Sevgen S, Samli R. A study on the hydrogen consumption calculation of proton exchange membrane fuel cells for linearly increasing loads: Artificial Neural Networks vs Multiple Linear Regression. Renewable Energy. 2020;156:570-8.

[35] Li Y, Li J, Huang J, Zhou H. Fitting analysis and research of measured data of SAW micro-pressure sensor based on BP neural network. Measurement. 2020;155:107533.

[36] Guo Y. Credit Risk Assessment of P2P Lending Platform towards Big Data based on BP Neural Network. Journal of Visual Communication and Image Representation. 2019:102730.

[37] Wang S, Wu TH, Shao T, Peng ZX. Integrated model of BP neural network and CNN algorithm for automatic wear debris classification. Wear. 2019;426-427:1761-70.

[38] Friedman JH. Multivariate Adaptive Regression Splines. Annals of Statistics.

1991;19(1):1-67.
[39] Qi X, Wang H, Pan X, Chu J, Chiam K. Prediction of interfaces of geological formations using the multivariate adaptive regression spline method. Underground Space. 2020.
[40] Chu W-x, Bennett K, Cheng J, Chen Y-t, Wang Q-w. Numerical study on a novel hyperbolic inlet header in straight-channel printed circuit heat exchanger. Applied Thermal Engineering. 2019;146:805-14.
[41] Zhao C, Yang J, Zhang T, Yan D, Pu J, Chi B, et al. Numerical modeling of manifold design and flow uniformity analysis of an external manifold solid oxide fuel cell stack. International Journal of Hydrogen Energy. 2020;45:14440-51.
[42] Kumaraguruparan G, Kumaran RM, Sornakumar T, Sundararajan T. A numerical and experimental investigation of flow maldistribution in a micro-channel heat sink. International Communications in Heat and Mass Transfer. 2011;38:1349-53.
[43] Riedmiller M, Braun H. A direct adaptive method for faster backpropagation learning: the RPROP algorithm. IEEE International Conference on Neural Networks1993. p. 586-91 vol.1.
[44] Elliott DL. A better activation function for artificial neural networks. Technical Research Report TR 93-8. 1993; Institute for Systems Research.
[45] Wu H-W, Gu H-W. Analysis of operating parameters considering flow orientation for the performance of a proton exchange membrane fuel cell using the Taguchi method. Journal of Power Sources. 2010;195:3621-30.

559 **Table 1**

560 Literature studies of PEMFCs with optimization methodology.

Major research focus	Optimization methodology	Important finding	Ref.
Using rectangular cylinders to Analyze the performance of PEMFCs in the channel under reasonable pressure drop.	Taguchi method	The maximum power density of the optimal configuration design parameters is 0.69 W cm^{-2}.	[11]
Optimization of design and operating parameters on the 25 cm^2 electrode surface active area of the PEMFC was carried out.	Taguchi method	The maximum power density for optimized parameters of PEMFC obtained by using Minitab 17 was 0.406 W/cm^2 and from the CFD model it was 0.408 W/cm^2.	[12]
Estimate the output voltage of PEM fuel cells.	Genetic algorithm neural networks, Taguchi method	Experiment results of PEMFC are employed to govern the factors' value for GANN model optimizing.	[13]
Analysis numerous parameters affecting the PEMFC performance.	Taguchi method, neural network	The operating temperature and pressure are the significant factors in affecting the PEMFC performance.	[17]
Estimate the optimal performance of an unknown proton exchange membrane fuel cell.	Taguchi method, generic numerical	The optimal output power of the PEMFC model is larger than that of the unknown PEMFC ((P_{model}) max ≥ (P_r) max).	[18]
Determines the optimal operating parameters for PEMFC stack to obtain small variation and maximum electric power output.	Taguchi method, neural network	The PEMFC stack is operated at the current densities of 0.4–0.8 A/cm^2. Since the voltage shift is quite small, the efficiency would be higher.	[19]
Finding the best combination of operation conditions of a PEM fuel cell.	Taguchi method	The amount of maximum power of the optimal combination factor is 17.61 W.	[45]

561

562 **Table 2**

563 Control factors and level settings for Taguchi method.

Factor	Control parameter	Level			
		1	2	3	4
A	Tube-to-IZ length ratio*	9.0	5.7	4.0	3.0
B	IZ width (mm)	14.0	15.0	16.0	17.0
C	Tube diameter (mm)	7.5	8.0	8.5	9.0

564 IZ*: Intermediate zones.

565

Table 3

Level combination of designed geometric dimensions in a L_{16} (4^3) orthogonal array.

Case	Factor		
	A	**B**	**C**
1	1	1	1
2	1	2	2
3	1	3	3
4	1	4	4
5	2	1	2
6	2	2	1
7	2	3	4
8	2	4	3
9	3	1	3
10	3	2	4
11	3	3	1
12	3	4	2
13	4	1	4
14	4	2	3
15	4	3	2
16	4	4	1

569 **Table 4**

570 Analysis of variance for the three factors.

Level	Factor			
	A		**B**	**C**
1	0.458215		0.455746	0.382661
2	0.456458		0.452346	0.427217
3	0.447858		0.453059	0.479729
4	0.448398		0.449779	0.521323
Factor	**Si**	**f**	**Deviation from mean sum of squares**	**F**
A	S_A=0.000346	3	0.000115	19.15
B	S_B=0.000072	3	0.000024	4.00
C	S_C=0.043978	3	0.014659	2434.73
Error	0.000072	12	0.000006	-

571
572

573 **Table 5**

574 Basis functions and corresponding equations of the MARS model.

BFs	Coefficient	Equations
BF_1	0.3831	max(0, A-7)
BF_2	-0.0028	max(0, 7-A)
BF_3	0.1572	max(0, B-7.83)
BF_4	-0.0451	max(0, 7.83-B)
BF_5	-0.0047	BF_1*max(0, C-14)
BF_6	0.0071	BF_2*max(0, B-8.5)
BF_7	0.0125	BF_2*max(0, 8.5-B)
BF_8	-0.0775	BF_3*max(0, B-8.5)
BF_9	-0.0479	max(0, 5-A)*max(0, 7.83-B)

575

576 **Table 6**

577 Comparison of pressure uniformity of three different methods

Factor	Method		
	Taguchi Method	**NN**	**MARS**
A	9.0	9.0	9.0
B	14.0	14.0	14.0
C	9.0	9.0	9.0
Predicted uniformity	-	0.520	0.549
Simulated uniformity	0.529	0.529	0.529
Relative error (%)	-	1.62	3.89

578
579

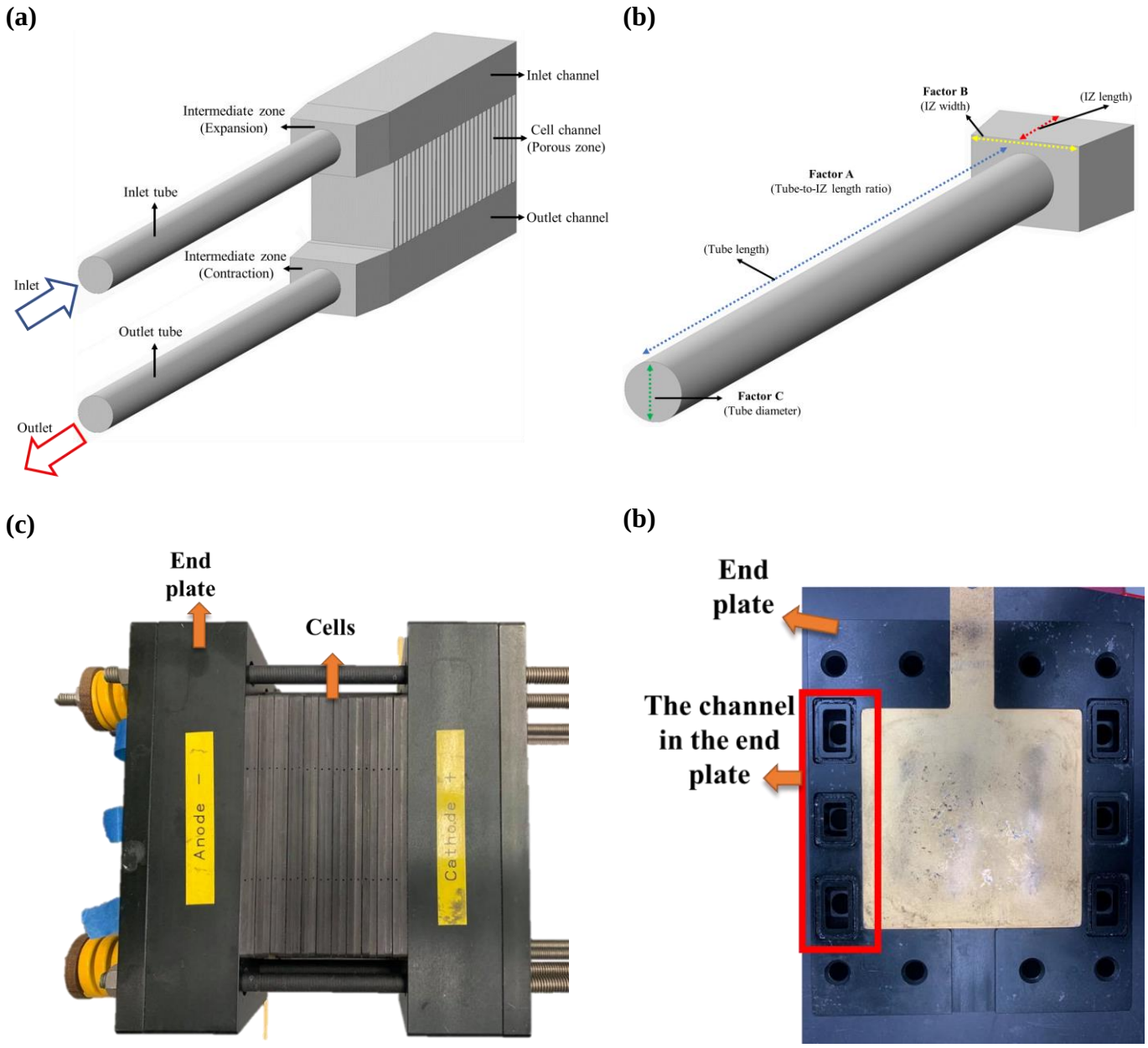

580 **Fig. 1.** Schematics of (a) physical configuration system and (b) geometric size of the fuel cell,

581 and (c) the end plate in the PEMFC and (d) the experiment configuration.

582

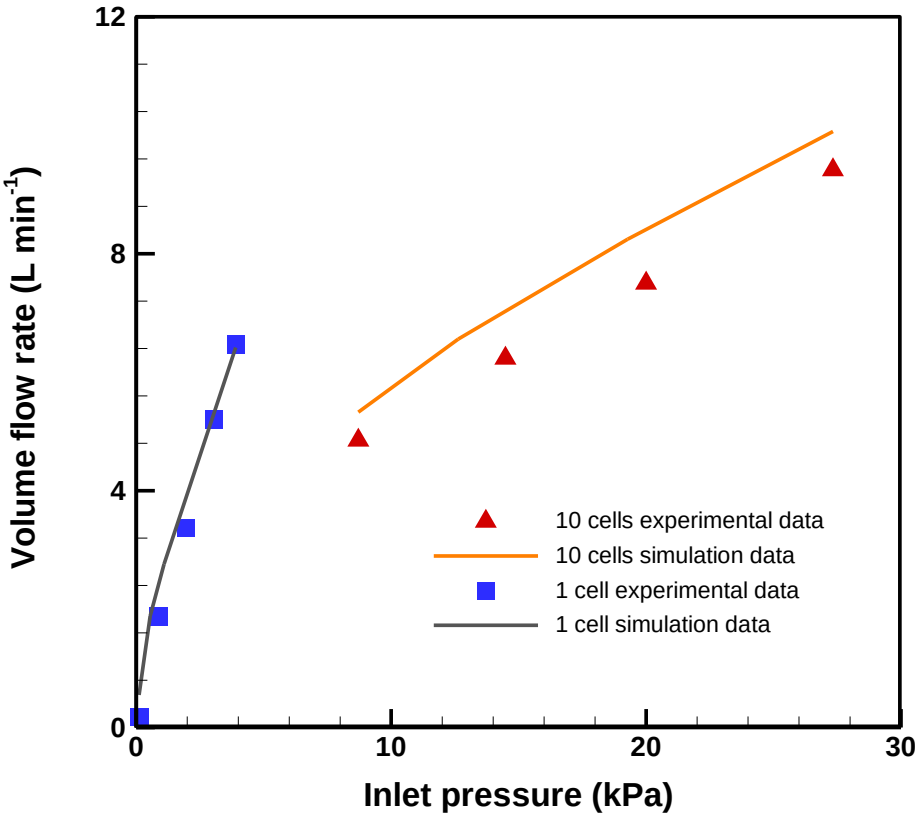

583
584 **Fig. 2.** Comparisons of simulation and experimental data of both cases of single-cell and 10-cell
585 stacks.
586

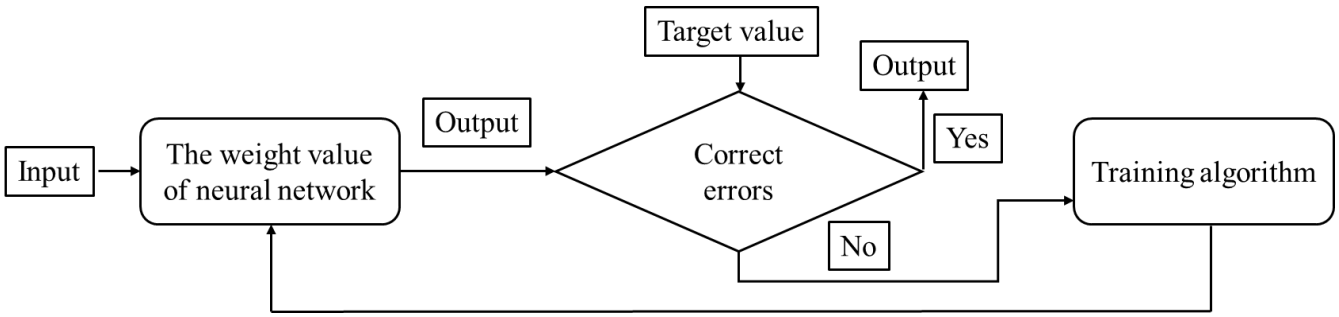

587

588 **Fig. 3.** Flow chart of NN training processes.

589

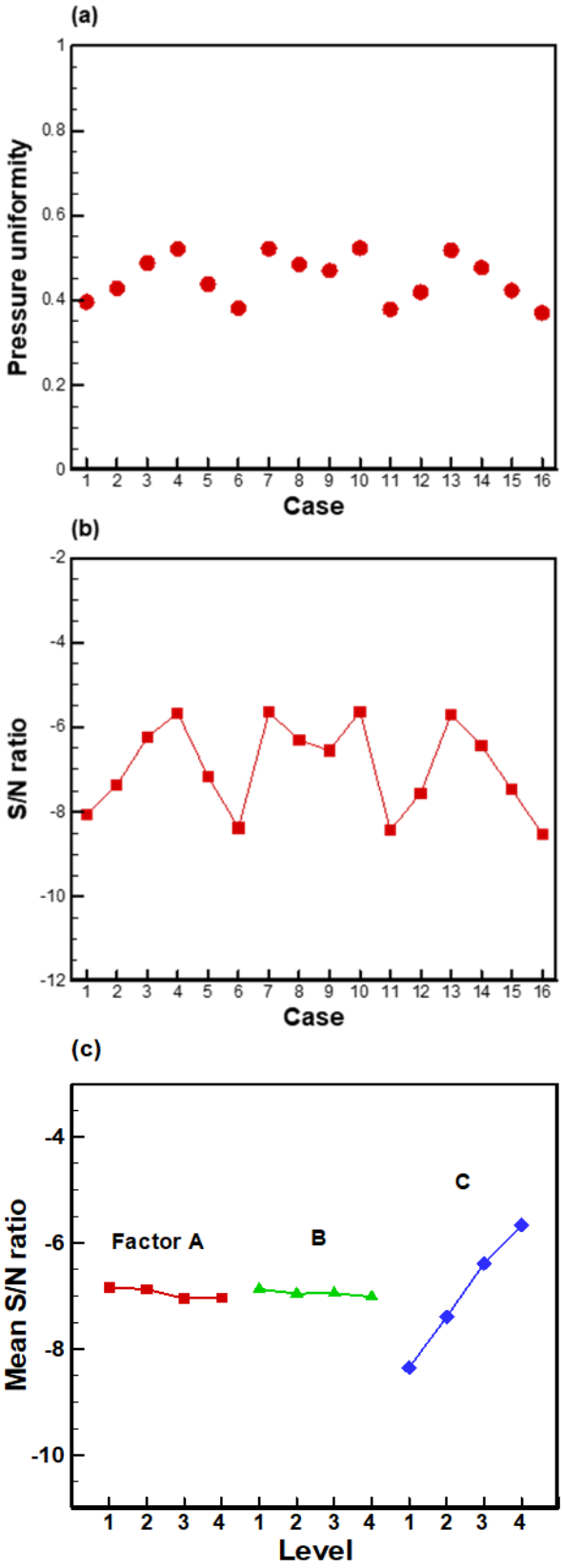

590

591 **Fig. 4.** Profiles of (a) pressure uniformity in 16 cases, (b) S/N ratio and (c) mean S/N ratios of

592 factors.

(a) Taguchi method

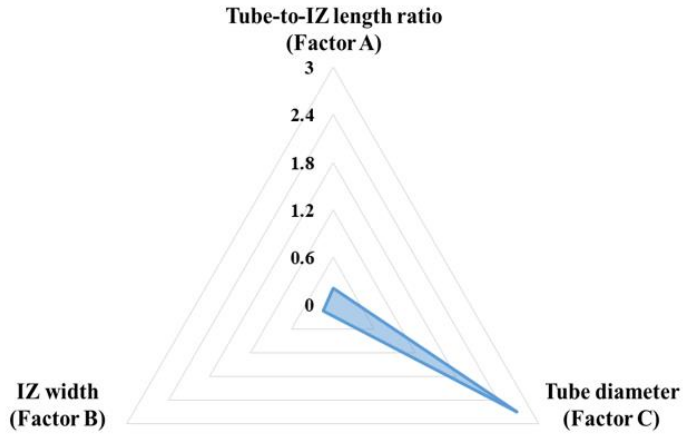

(b) NN

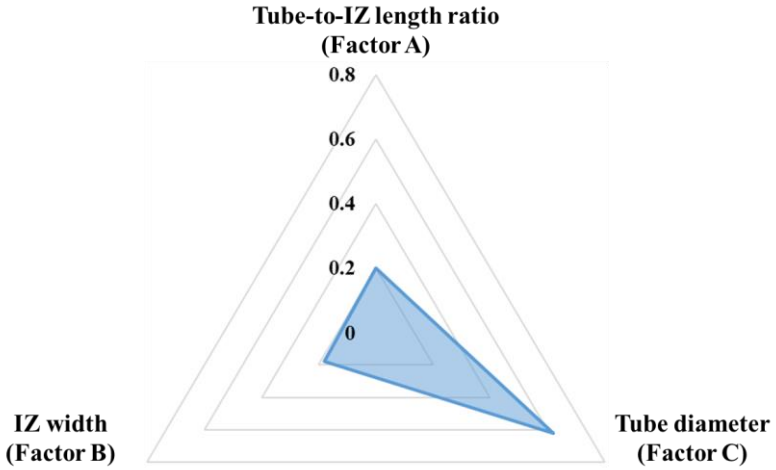

(c) MARS

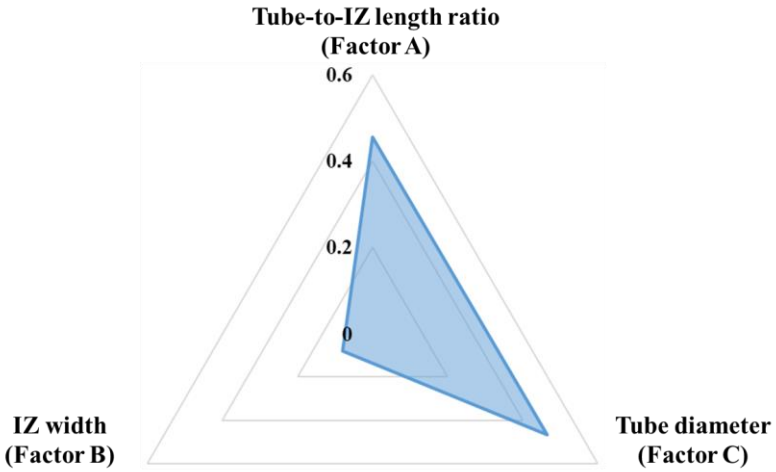

593 **Fig. 5.** Radar charts of effect of factors in (a) Taguchi method, (b) NN, and (c) MARS.

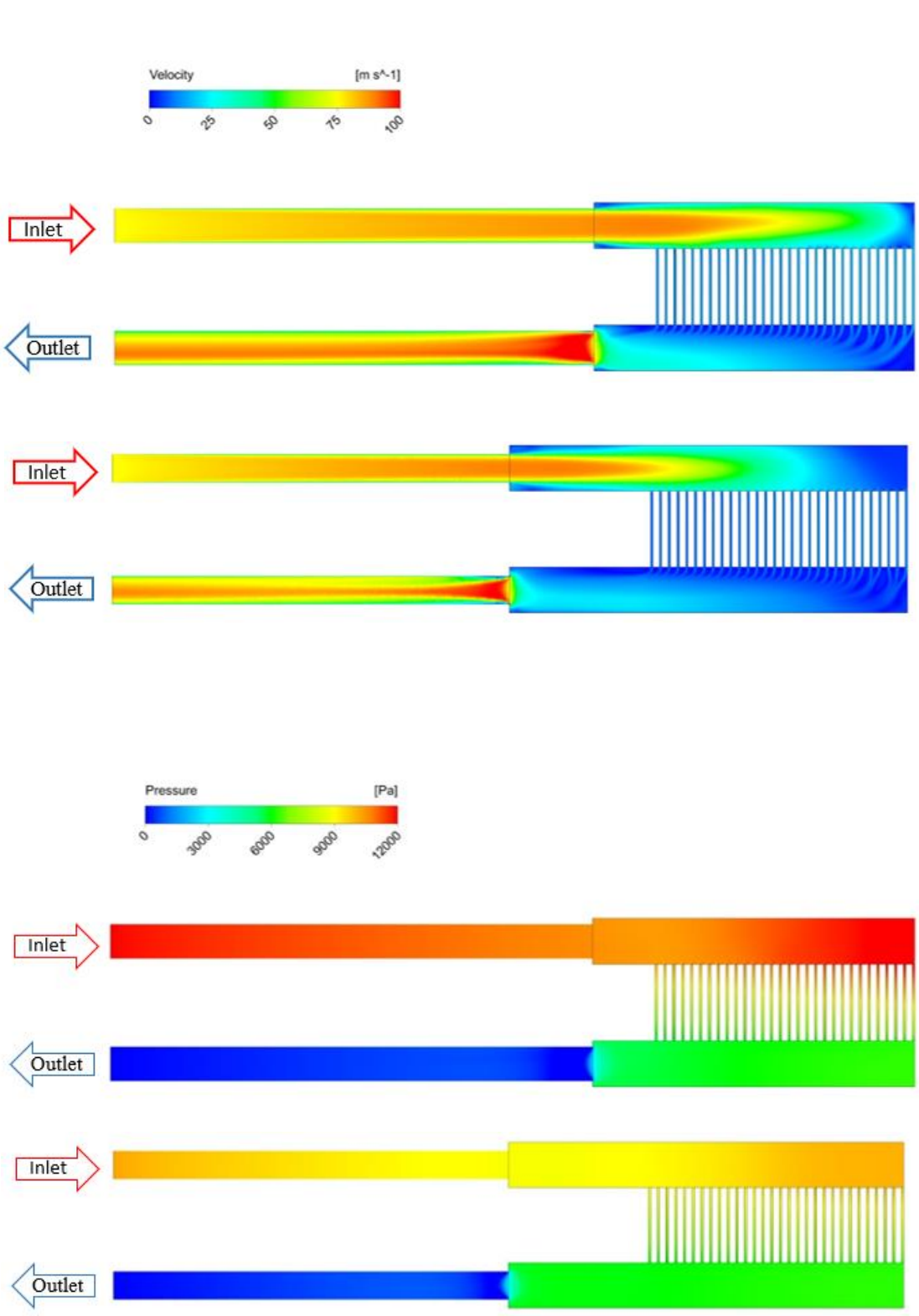

Fig. 6. Velocity contours of (a) the optimal case and (b) Case 16, and pressure contours of (c) the optimal case and (d) Case 16.

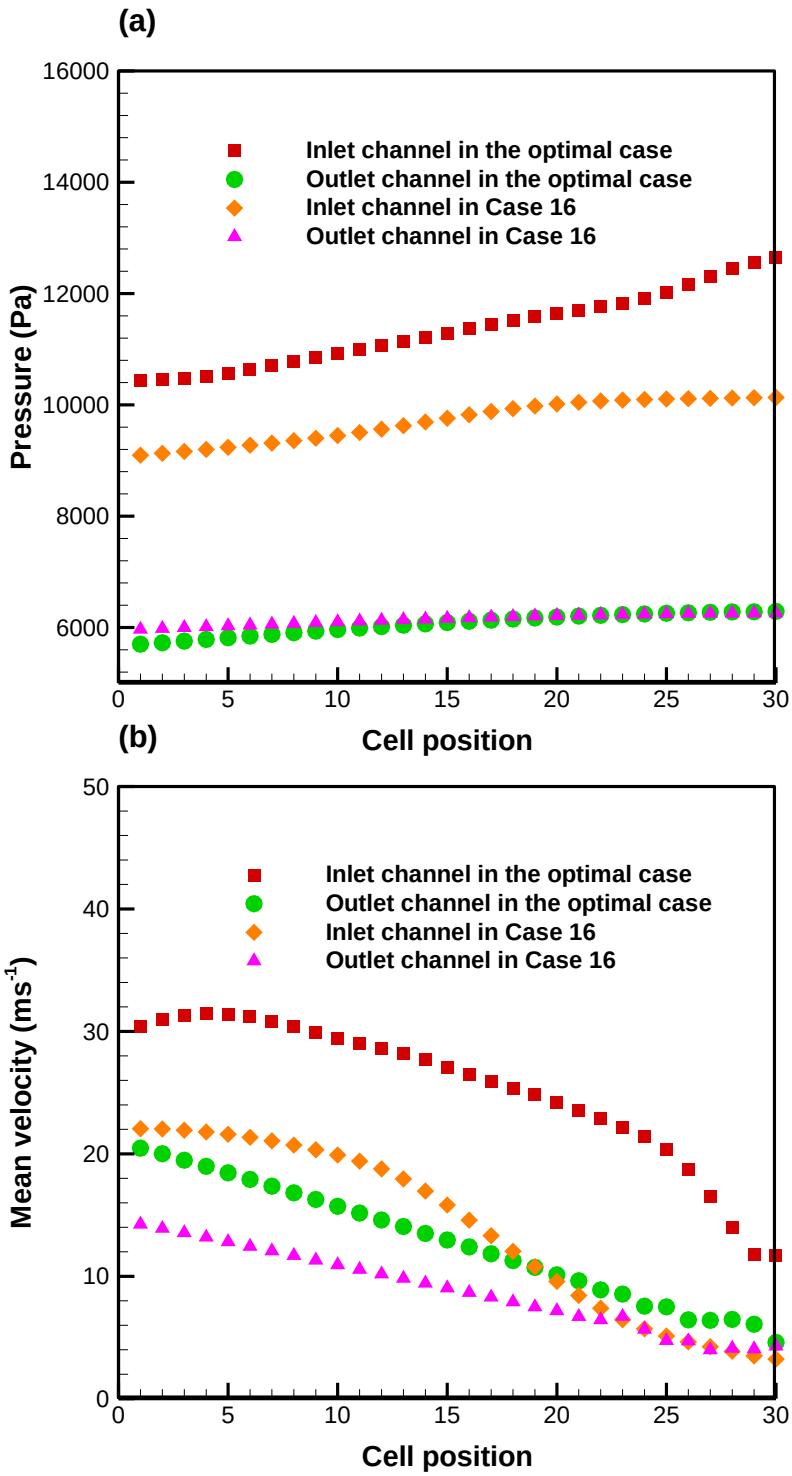

596

597 **Fig. 7.** Profiles of (a) pressure and (b) mean velocity along the inlet and outlet channel with the

598 optimal combination and Case 16.

599

(a)

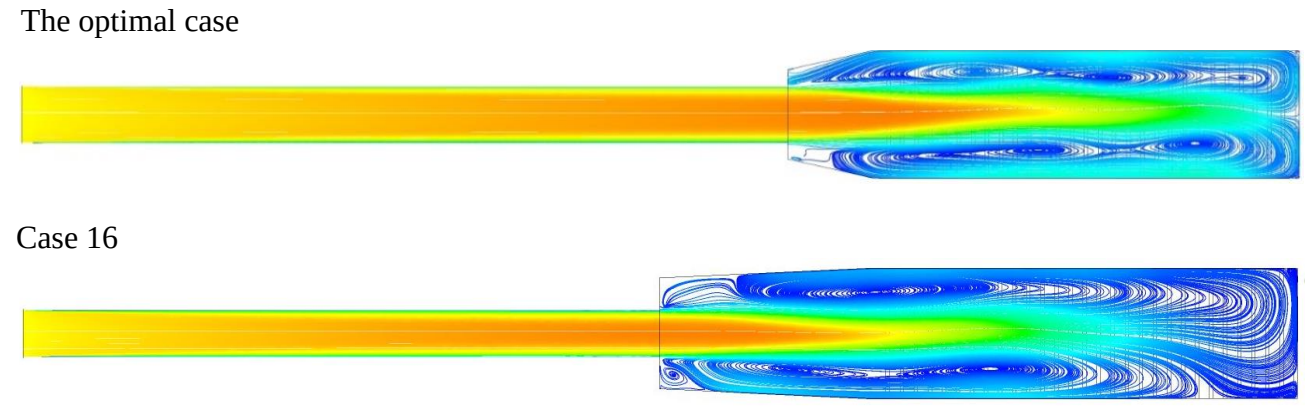

(b)

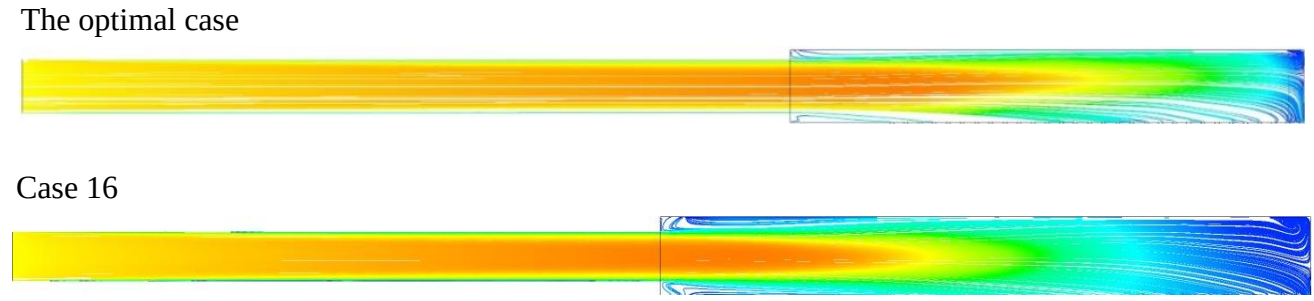

600 **Fig. 8.** Visualization of streamline of inlet channel: (a) top view, (b) side view.

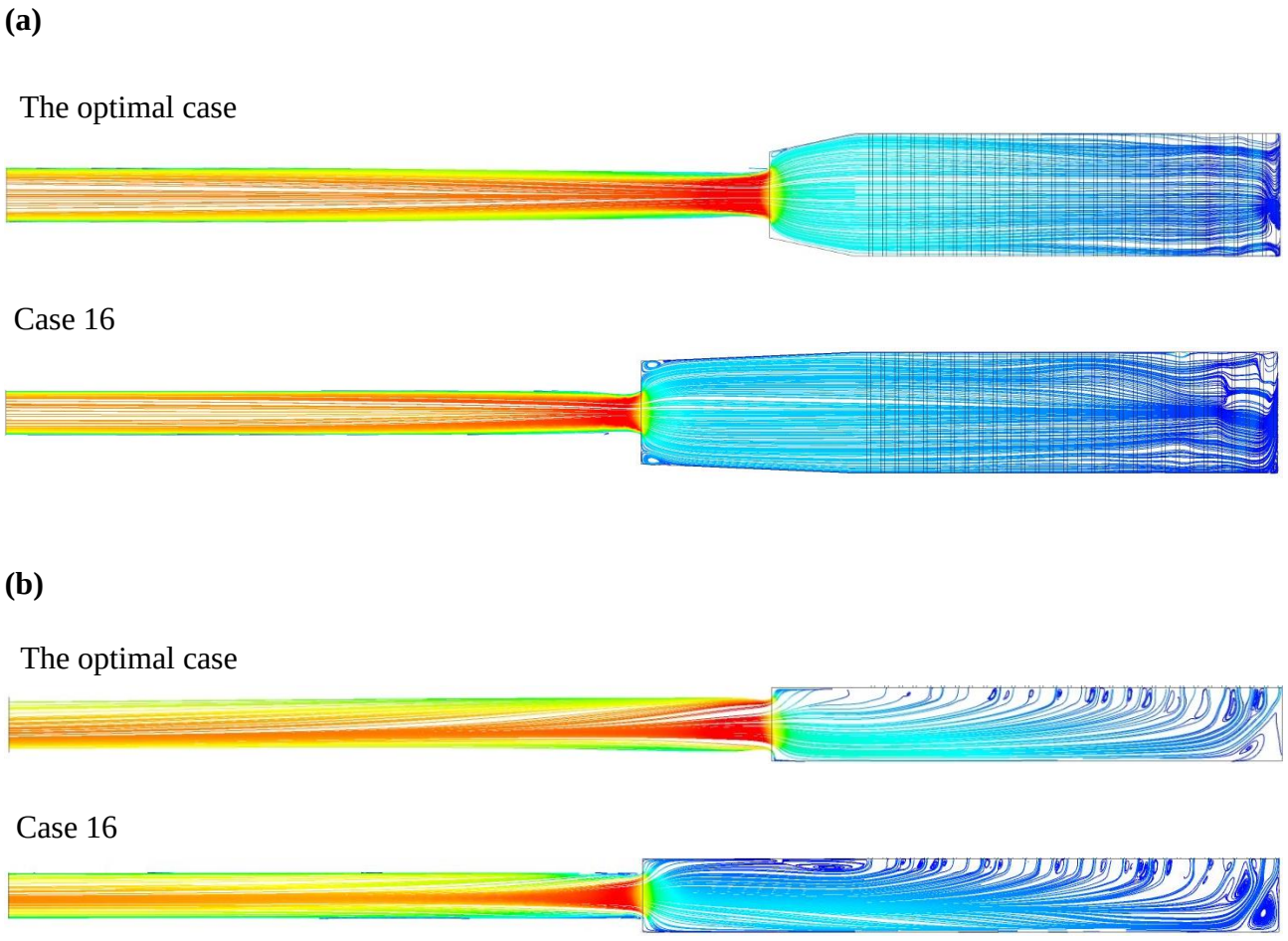

Fig. 9. Visualization of streamline of outlet channel: (a) top view, (b) side view.

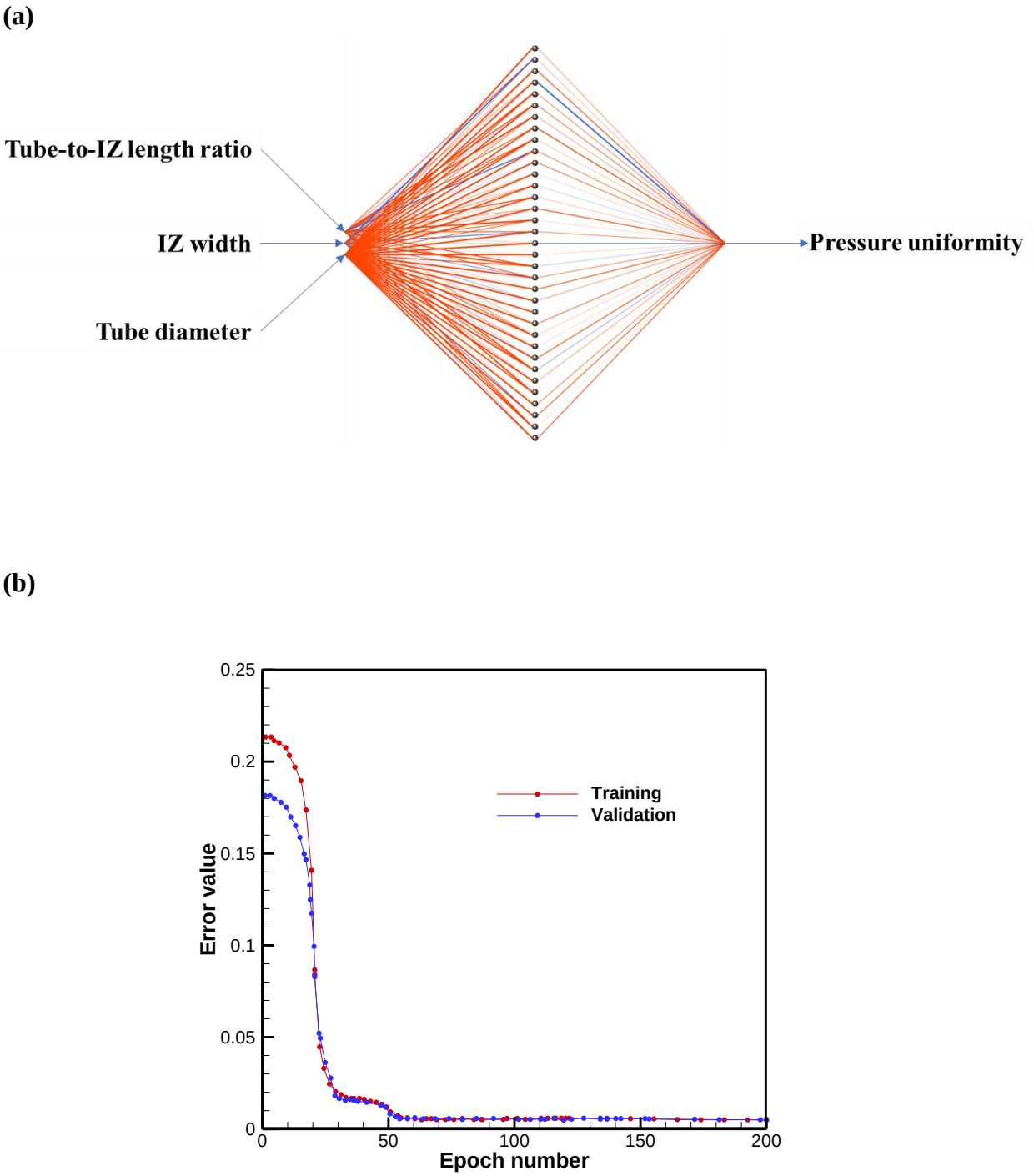

603 **Fig. 10.** (a) Visualization structure and (b) profiles of error value between training and validation
604 data in neural network.
605

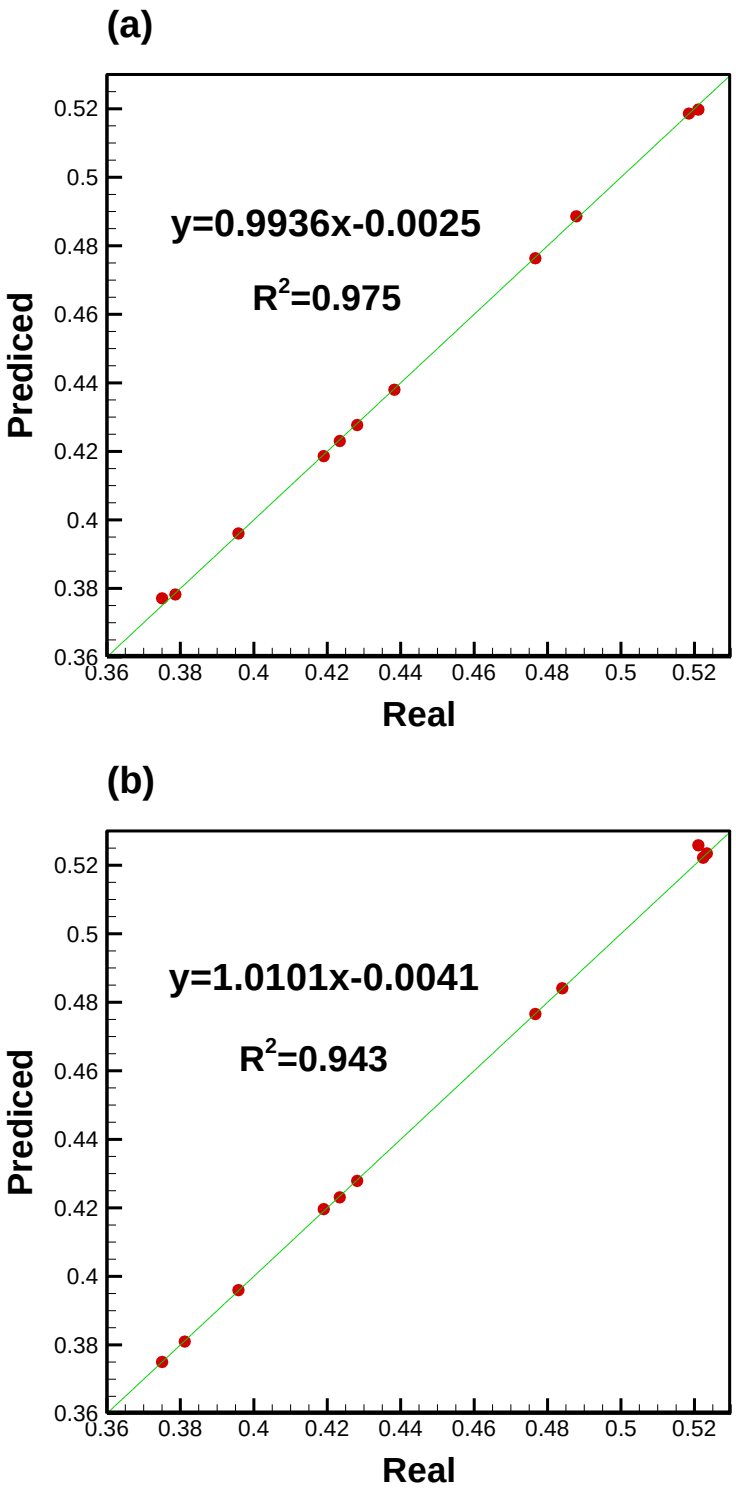

606

607 **Fig. 11.** Regression analysis between predicted and real value in (a) NN and (b) MARS.

608

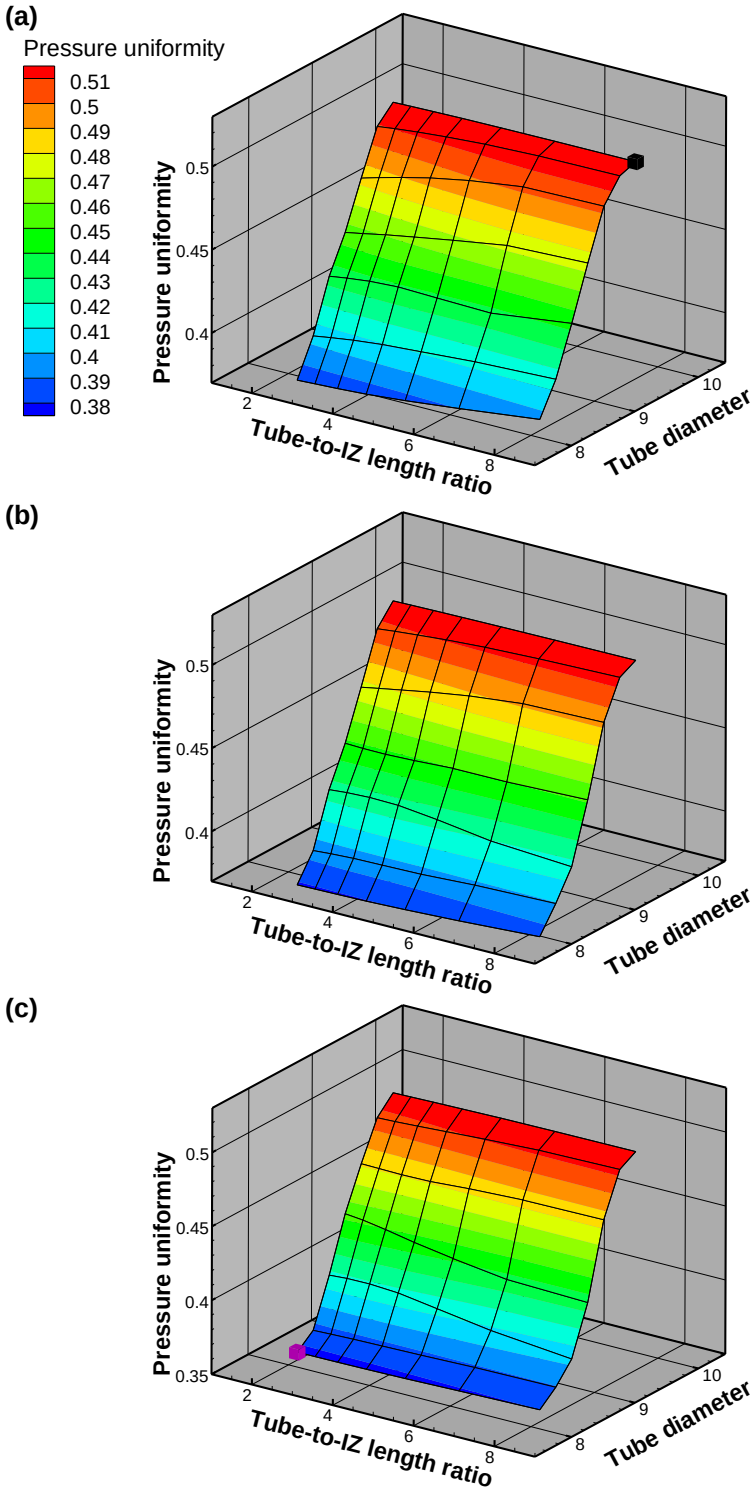

609

610 **Fig. 12.** Three-dimensional distributions of pressure uniformity in NN when the IZ width is fixed

611 at (a) 14, (b) 15.5, and (c) 17 mm.

612

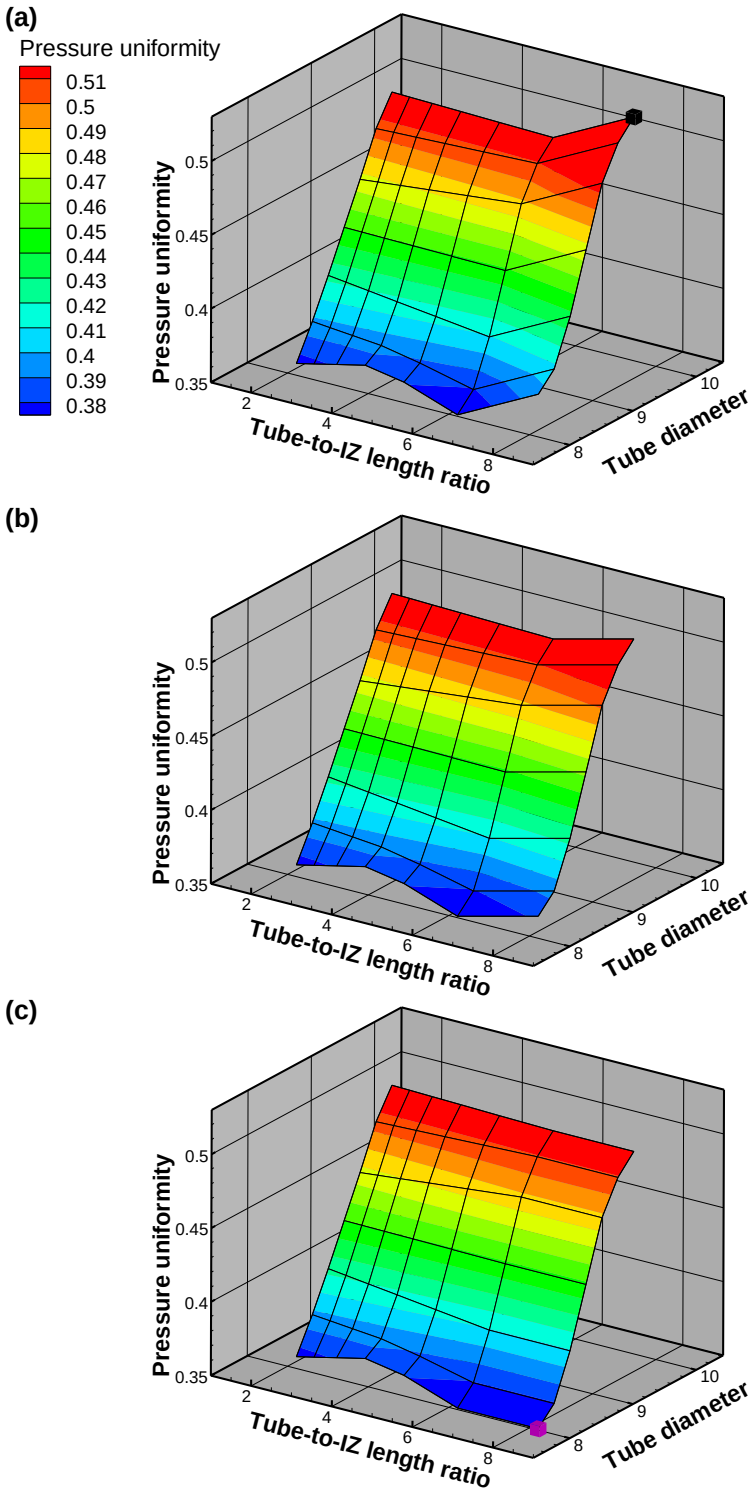

Fig. 13. Three-dimensional distributions of pressure uniformity in MARS when the IZ width is fixed at (a) 14, (b) 15.5, and (c) 17 mm.